Compensation of seeding bias for particle tracking velocimetry in turbulent flows

Thomas Barois, Bianca Viggiano, Thomas Basset, Raúl Bayoán Cal, Romain Volk, Mathieu Gibert, Mickaël Bourgoin

Editors' Suggestion

Compensation of seeding bias for particle tracking velocimetry in turbulent flows

Thomas Barois,[1] Bianca Viggiano,[2] Thomas Basset,[3] Raúl Bayoán Cal,[2] Romain Volk,[3] Mathieu Gibert,[4] and Mickaël Bourgoin[3]

[1]*Univ. Bordeaux, CNRS, LOMA, UMR 5798, F-33400 Talence, France*

[2]*Department of Mechanical and Materials Engineering, Portland State University, Portland, Oregon 97201, USA*

[3]*Ens de Lyon, CNRS, Laboratoire de physique, UMR 5672, F-69342 Lyon, France*

[4]*Univ. Grenoble Alpes, CNRS, Grenoble INP, Institut Néel, 38000 Grenoble, France*

(Received 9 March 2023; accepted 13 June 2023; published 19 July 2023)

When a fluid in turbulent motion is tagged by a nonuniform concentration of ideal tracers, the mean velocity of the tracers may not match with the mean velocity of the fluid flow. This implies that conventional particle tracking velocimetry will not produce the mean flow of a turbulent flow unless the particle seeding is homogeneous. In this work, we consider the problem of mean flow estimation from a set of particle tracks obtained in a situation of nonhomogeneous seeding. To compensate the bias caused by the nonhomogeneous particle seeding, we propose a modified particle tracking velocimetry method. This method is called a time-delayed velocity and considers the velocity trajectory of a given particle shifted in time with respect to its position. We first introduce our method for an ideal advection–diffusion model and then we implement it for a turbulent channel and a turbulent jet. For both situations, we find that the velocity bias caused by the nonhomogeneous tracer concentration is reduced with a time delay introduced between position and velocity of the tracer trajectories. For the turbulent channel, the error on the mean flow estimation monotonically decreases for increasing time delays. For the turbulent jet, the error on the mean flow estimation also reduces with positive time delays but the time delay should not be too large. We interpret this limitation as a consequence of the spatial dependence of the mean flow. For the turbulent channel, this limitation does not appear because the velocity for the mean flow streamlines is constant. For both flows, the optimal time delay for the velocity bias compensation is consistent with the Lagrangian timescales of the flow. This method gives promising elements to take into account inhomogeneous seedings in velocity fields measurements for all kinds of turbulent flows and interesting perspectives to understand how Lagrangian trajectories from various sources build an Eulerian mean field.

DOI: 10.1103/PhysRevFluids.8.074603

I. INTRODUCTION

Among the strategies to measure the velocity of a flowing fluid, particle image velocimetry (PIV) [1–3] and particle tracking velocimetry (PTV) [4–8] are two techniques that rely on the dispersion of a large number of particles in the fluid. To behave as nonintrusive tracers that correctly map the flow, the particles should be sufficiently small [9,10] and neutrally buoyant [11]. In addition to the physical properties of the tracing particles, the homogeneity of the particle concentration [12–14] is also important to produce reliable flow measurements. With a nonhomogeneous seeding, the particle concentration may be too low in some regions of the fluid, which renders the measurement spatially incomplete.

The homogeneity of the tracing particles has a direct impact on the estimation of the mean velocity of a flow. With the example of turbulent jets with particles injected from the nozzle, there is a significant mismatch between the measured radial velocities from the particle tracking analysis and the expected radial velocities [14]. In recent a work [15], it was shown that this radial velocity mismatch is consistent with the particle dispersion by the turbulent jet which can be formulated as a compressible expansion flow for the tracers resulting in an enhanced radial flow.

For laminar flows without velocity fluctuations, homogeneous and nonhomogeneous seedings provide the same mean flow velocity. This is because without velocity fluctuations, the particles consistently follow the time-independent streamlines of the flow. The absence of velocity fluctuations is however not ideal for flow visualization since there is no particle dispersion perpendicularly to the stationary streamlines. This problem notably occurs with microfluidics [16,17] in which the dispersion of tracers, i.e., mixing, is notoriously inefficient.

To address how turbulence and inhomogeneous seeding can induce mean flow bias by particle tracking, a first example is that of molecular diffusion which is a well-known situation in which particle inhomogeneity can affect mean flow perception. For a fluid at rest with diffusing particles, there is a mismatch between the zero mean velocity of the fluid and the particles velocity everywhere nonzero concentration gradients exist. The velocity of Brownian particles is however difficult to measure and the diffusion current is rather inferred from the concentration time evolution of the diffusing particles. In a turbulent flow, fluctuations induce an effective diffusion process [18] that is much more efficient than molecular diffusion. For comparison, the molecular diffusion coefficient in a fluid is $K_{\mathrm{mol}} \propto v_{\mathrm{th}}\ell$ in which v_{th} is the thermal velocity and ℓ the molecular mean free path. The typical order of magnitude for K_{mol} for fluids such as water is 10^{-9} m^{2}s^{-1} for ambient pressure and room temperature. In turbulent flows, an effective diffusion coefficient $K_{\mathrm{turb}} \propto \sigma_v \mathcal{L}$ arises from the velocity fluctuation magnitude σ_v and the typical size $\mathcal{L}$ of the largest eddies of the considered flow. For laboratory-scale experiments such as turbulent channels [19,20], the diffusion coefficients can be of the order of 10^{-4} m^{2}s^{-1}. In atmospheric turbulence [21–24], the turbulent diffusion coefficient can easily reach 1 m^{2}s^{-1}. In this work, we consider more specifically the configurations of turbulent channels and turbulent jets and we will illustrate how turbulent fluctuations combined with non homogeneous particle seeding can lead to significant mean velocity biases in particle tracking velocimetry.

In principle, it is always possible to reduce the impact of turbulent fluctuations on mean flow measurements by approaching a homogeneous concentration of tracers. However, it is not always possible or convenient to perform a homogeneous seeding. This is the case for experiments in open environment like oceanic or atmospheric studies [25–27] in which uniform seeding can be difficult to control, even for a finite volume of interest. For laboratory experiments in fluid tanks, for example, partial seeding is sometimes preferred to avoid too many particles in the field of view. This is notably the case for the realization of unconfined turbulent jets for which the tank has to be much larger than the jet size. In some situations, the particles can have a finite life-time, like soap bubbles [28,29] or droplets [30,31], and seeding concentration is very difficult to control. With bubbly flows [32–34], the bubbles can be used as nonideal tracers but their concentration is difficult to maintain constant because the bubble formation, recombination, shape and disappearance is self-imposed by the flow itself. Finally, nonhomogeneous particle concentration can occur because of clustering induced by the flow. This particularly happens with particles in sedimentation [35] as well as inertial particles in turbulent flows [36–39].

The goal of this work is first to illustrate how tracer inhomogeneity affects the determination of mean velocity fields and second to present a simple analysis technique to obtain unbiased velocity fields in the case of tracking experiments with nonhomogeneous seeding.

II. DISCRETE ADVECTION-DIFFUSION MODEL

A. Lagrangian and Eulerian perspectives

This work deals with the velocity estimation of flows (Eulerian perspective) based on the observation of a set of tracers moving in a fluid (Lagrangian perspective). In the Eulerian framework, the

instantaneous velocity $v_i(x, y, z, t)$ is a three-component function with $i = x, y$ or z that represents all the velocity information of a flow at any position (x, y, z) and time t. The mean velocity identified by uppercase $V_i(x, y, z)$ is the time-average of the fluid velocity $v_i(x, y, z, t)$ at a given location in space (Eulerian perspective). Because we will address the problem of partial seeding, we should stress on the fact that the computation of the mean velocity $V_i(x, y, z)$ rigorously requires that all the fluid particles that pass at the vicinity of the location (x, y, z) are taken into account in the time-averaging operation.

With tracing particles, only a small portion of the flow is tagged in terms of volume fraction. We note $\phi(x, y, z)$ the time-averaged tracer concentration of injected particles. For each location (x, y, z) in the flow domain, we define the tracer mean velocity $\mathcal{V}_i(x, y, z)$ (Lagrangian perspective) which is the time-averaged velocity of all the tracers passing at (x, y, z) during the acquisition time. For a homogeneous tracer concentration with $\phi(x, y, z) = \phi_0$ independent of space, the tracer mean velocity is also the mean flow velocity $\mathcal{V}_i(x, y, z) = V_i(x, y, z)$ and there is no need to make a distinction between fluid mean velocity and tracer mean velocity. For a nonhomogeneous tracer concentration, $\mathcal{V}_i(x, y, z)$ and $V_i(x, y, z)$ are *a priori* different. The origin of the difference between $\mathcal{V}_i(x, y, z)$ and $V_i(x, y, z)$ is illustrated and discussed in more detail in the following section. We should specify that $\mathcal{V}_i(x, y, z)$ and $V_i(x, y, z)$ could also differ because of nonideal tracers. With finite-size tracers or nonperfect density matching, the velocity of the tracers may not correspond to the velocity of the surrounding fluid. However, we will consider in this work that the bias caused by possibly nonideal tracers is negligible and the bias caused by nonhomogeneous seeding dominates.

The main point of this work is to discuss a method to retrieve the mean velocity of the flow $V_i(x, y, z)$ from the analysis of tracer trajectories when $\mathcal{V}_i(x, y, z) \neq V_i(x, y, z)$ because of nonhomogeneous particle concentration. To do so, we will introduce in the next section a so-called time-delayed velocity $\mathcal{V}_i(x, y, z|\Delta\tau)$ in which $\Delta\tau$ is an adjustable parameter corresponding to the time delay.

B. Toy model

Before considering realistic turbulent flows with injected tracers, a simple toy model of advection-diffusion is presented. The point of this toy model is first to illustrate how nonhomogeneous seeding impacts the estimation of mean flows and second to present the method we propose to compensate the seeding bias. In this two-dimensional model, the mean flow is $V_x(x, z) = 0$ and $V_z(x, z) = v_0$.

We consider the dynamics of pointlike particles in a two-dimensional space with a uniform mean advection in the axial direction and submitted to transverse diffusion. The particles are initially at the origin of the frame $x = 0$ and $z = 0$ and move by steps. The motion in the axial direction z accounts for a pure advection and the particles move by constant unit step $+1$ for each time step. For the transverse direction x, no advection is imposed and the average velocity of the background flow is zero. However, the individual particles do diffuse according to the simple process where at each time step, each particle has an equal probability to jump either left $(-1/2)$ or right $(+1/2)$. With a homogeneous seeding, this process with equal probability of motion to the left and to the right does not impose any mean transverse flow. Figure 1(a) represents all the possible trajectories for eight particles after three time steps. While the actual advecting velocity is a uniform upward flow, we illustrate the bias introduced by the nonhomogeneous seeding by considering the flow tagged by the particles seeded at the origin in the square box represented with a dashed line in Fig. 1(a). For the three particles in the binning box, two particles come from the left and one particle comes from the right. After multiple iterations of the random process for a set of particles, one should expect a net positive horizontal velocity for the particles reaching the considered box.

To test the large trajectory number limit, we numerically generate the trajectories for a large number of particles. Figure 1(b) shows the Eulerian velocity field obtained from a set of trajectories generated randomly according to the discrete process described above and represented in Fig. 1(a). A total number of 2×10^5 trajectories were simulated to explore a significant portion of horizontal

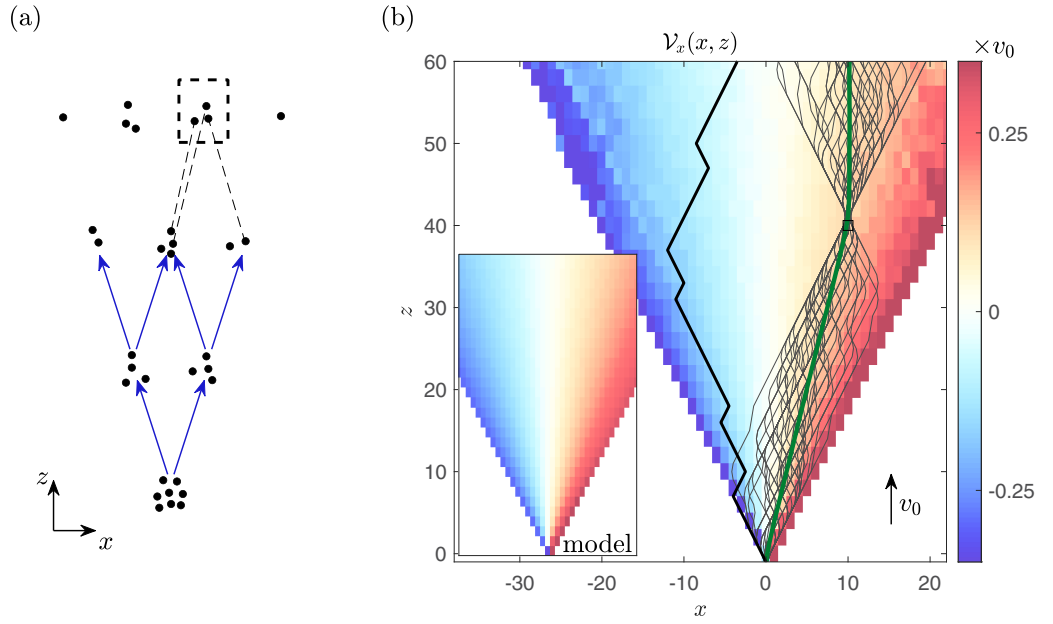

FIG. 1. (a) Representation of a step-by-step process with 8 particles moving vertically with a horizontal fluctuating motion left and right for each time step. (b) Eulerian contour obtained after multiple iterations of the step-by-step process with random jumps and an averaging of the trajectories in a binning grid (2×10^5 trajectories in total). The color scale indicates the mean horizontal velocity $\mathcal{V}_x$ of the simulated trajectories. A subset of trajectories passing by both bins $\{0, 0\}$ and $\{x = 10, z = 40\}$ are represented by solid lines. A thick green line represents the average trajectory from this subset. Another trajectory exploring $x < 0$ is also represented. The inserted contour is the model for the horizontal velocity presented in Eq. (8).

space. The black solid line represents a random sample trajectory exploring the $x < 0$ region. The average velocity retrieved from the seeded tracers strictly matches the average velocity of the fluid for the injection line $x = 0$. Elsewhere, the horizontal velocity is however positively (for $x > 0$) or negatively (for $x < 0$) biased. For the large $|x|$, there are very few trajectories and thus a lack of statistical convergence. This velocity bias is a direct consequence of the local seeding. For uniform seeding, i.e., a constant concentration of particles on the line $z = 0$, the horizontal velocity vanishes within statistical convergence.

The origin of the velocity bias can be better visualized by considering a subset of trajectories that pass by the bin $\{x = 10, z = 40\}$ represented by a small box with a dashed line in Fig. 1(b). For a total of 2×10^5 simulated trajectories, there is typically a number of 500 trajectories that reach the bin considered [Fig. 1(b) only represents 30 of those trajectories for clarity]. In the figure, a green solid line is used to represent the mean path for all the trajectories passing by the binning box $\{x = 10, z = 40\}$. If a reference time is taken when the particles reach the box, then there is an asymmetry between past and future. Before the particles enter the bin, there is a positive velocity bias. This is because the most probable path for the particles coming from $x = 0, z = 0$ to reach the binning box is with an excess of positive jumps in x. After the particles have passed the bin $\{x = 10, z = 40\}$, there is no bias on the trajectories subset and the particle motion is mostly vertical as shown by the mean trajectory for $z > 40$.

The concentration ϕ and the horizontal component of the velocity $\mathcal{V}_x$ for the particles in this toy model can be analytically solved using the properties of Pascal's triangle. The process described in Fig. 1(a) leads to a continuity equation for the particles concentration $\phi(i, n) = [\phi(i, n - 1) + \phi(i - 1, n - 1)]/2$ in which n is the index for z and i is the index for the x direction with $0 \leqslant i \leqslant n$.

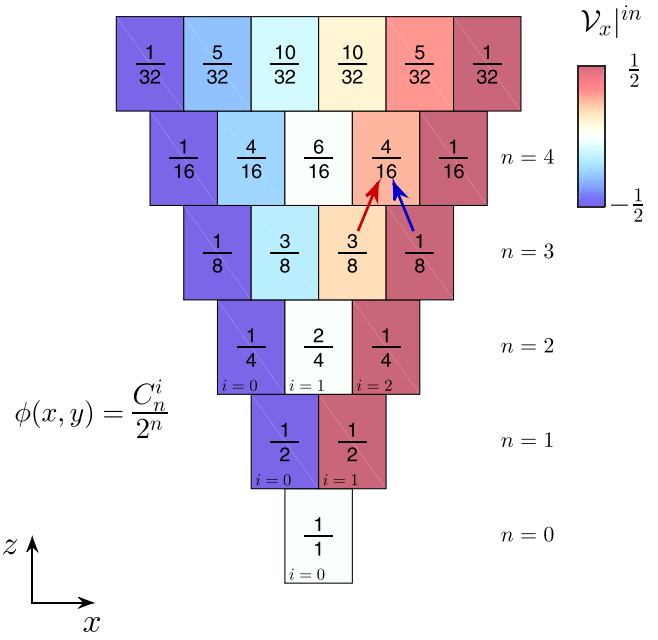

FIG. 2. Concentration profile $\phi(x, y)$ (expressed as a fraction) of the toy model in the limit of statistical convergence. i and n are positive integers ($i \leqslant n$), with $x(i, n) = i - n/2$ and $z(i, n) = n$. The particles start from $i = 0$, $n = 0$ and for each iteration, the particles move up with an equal probability $1/2$ to jump left or right. The colorbar indicates the value for the horizontal incoming velocity $\mathcal{V}_x|^{\text{in}}$ [Eq. (2)]. The two arrows illustrate the origin of the biased velocity $\mathcal{V}_x|^{\text{in}}$ at $n = 4$, $i = 3$ with a ratio 3:1 for the incoming particles from cells $i = 2$, $n = 3$ ($\phi = 3/8$, contributing to a positive horizontal velocity represented with a red arrow) and $i = 3$, $n = 3$ ($\phi = 1/8$, contributing to a negative horizontal velocity represented with a blue arrow).

This relation is equivalent to the definition of the binomial coefficient C_n^i with $\phi(i, n) = C_n^i/2^n$. The first steps of the iteration is presented in Fig. 2. The iteration for $n = 4$, $i = 3$ is represented by a set of boxes with $\phi(i = 3, n = 4) = 4/16$ as the sum from the contribution $1/2 \times (3/8 + 1/8)$ of the previous iteration.

For the transverse velocity, it is important to make a distinction between the incoming velocity $\mathcal{V}_x(i, n)|^{\text{in}}$ and the outgoing velocity $\mathcal{V}_x(i, n)|^{\text{out}}$ relatively to a given position. $\mathcal{V}_x(i, n)|^{\text{in}}$ is the velocity at step n using the position n and $n - 1$. $\mathcal{V}_x(i, n)|^{\text{out}}$ is the velocity at step n using the position n and $n + 1$. For a large number of realizations, the transverse outgoing velocity statistically converges to $\mathcal{V}_x(i, n)|^{\text{out}} = V_x(i, n) = 0$ because the particles equally moves left and right relatively to a given position. For the incoming velocity $\mathcal{V}_x(i, n)|^{\text{in}}$, the net transverse velocity is the weighted concentration contribution from the previous steps,

$$\mathcal{V}_x(i, n)|^{\text{in}} = \frac{\frac{v_0}{2} \times \phi(i-1, n-1) - \frac{v_0}{2} \times \phi(i, n-1)}{\phi(i-1, n-1) + \phi(i, n-1)} = \frac{v_0}{2} \frac{\phi(i-1, n-1) - \phi(i, n-1)}{\phi(i-1, n-1) + \phi(i, n-1)}, \quad (1)$$

in which $\phi(i - 1, n - 1)$ counts the number of particles per unit time coming from the left with velocity $+v_0/2$ and $\phi(i, n - 1)$ from the right with velocity $-v_0/2$ (the values for ϕ with $n = 4$ and $i = 3$ are $3/8$ and $1/8$ in the example of Fig. 2).

Equation (1) can be written as

$$\mathcal{V}_x(i, n)|^{\text{in}} = \frac{v_0}{2} \frac{C_{n-1}^{i-1} - C_{n-1}^i}{C_n^i} = v_0 \frac{i - \frac{n}{2}}{n}. \quad (2)$$

For a symmetric representation of Pascal's triangle in (xz), we use the variable $x(i,n) = i - n/2$ and $z(i,n) = n$. The incoming transverse velocity becomes

$$\mathcal{V}_x(x,z)|^{\text{in}} = \frac{x}{z} v_0. \tag{3}$$

From Eq. (3), we can infer the expression for the mean trajectory $X|_{x,z}, Z|_{x,z}$ for the subset of all particles injected at $\{0,0\}$ at $t = 0$ and passing in the bin $\{x, z\}$ at time $t = z/v_0$. An example of a mean trajectory $X|_{x,z}, Z|_{x,z}$ is represented by a green solid line in Fig. 1(b) for the bin $\{x = 10, z = 40\}$. For $t < z/v_0$, the particles move in average at a constant velocity from 0 to x as

$$X|_{x,z}(t) = \frac{x}{z} v_0 t \quad (t < z/v_0). \tag{4}$$

At $t = z/v_0$, the particles are in the bin $\{x, z\}$. For $t \geqslant z/v_0$, the average position for the particle passing by $\{x, z\}$ is

$$X|_{x,z}(t) = x \quad (t \geqslant z/v_0). \tag{5}$$

We can mention that the mean trajectory for $\{x = 10, z = 40\}$ represented by the thick green line in Fig. 1 is consistent with the expression for $X|_{x,z}(t)$ in Eqs. (4) and (5).

We show here that the local seeding at {0,0} leads to a biased mean trajectory for $t < z/v_0$ [Eq. (4)] and not for $t > z/v_0$ [Eq. (5)]. To compensate this bias, we introduce the time-delayed velocity for the horizontal component of the velocity,

$$\mathcal{V}_x(x,z|\Delta\tau) = \frac{X|_{x,z}(t + \Delta\tau + \delta t) - X|_{x,z}(t + \Delta\tau - \delta t)}{2\delta t}, \tag{6}$$

in which $t = z/v_0$ is the time for which the particle is at z, $\Delta\tau$ the time delay and δt the time increment from steps n to $n + 1$. Equation (6) with $\Delta\tau = 0$ is the usual two-point velocity estimation corresponding to $\mathcal{V}_x(i,n|0) = (\mathcal{V}_x(i,n)|^{\text{in}} + \mathcal{V}_x(i,n)|^{\text{out}})/2$. From the mean trajectory in Eqs. (4) and (5), the time-delayed velocity in Eq. (6) gives

$$\mathcal{V}_x(x,z|\Delta\tau < 0) = \frac{x}{z} v_0, \tag{7}$$

$$\mathcal{V}_x(x,z|\Delta\tau = 0) = \frac{1}{2}\frac{x}{z} v_0, \tag{8}$$

$$\mathcal{V}_x(x,z|\Delta\tau > 0) = 0. \tag{9}$$

Equation (7) is for a negative time delay which means that the velocity is computed with the track positions before the bin $\{x, z\}$. This velocity is the incoming velocity in Eq. (3). $\mathcal{V}_x(x,z|\Delta\tau < 0)$ is biased because the particles are injected at $\{0,0\}$ and to reach the bin $\{x, z\}$, there is a sampling bias in favor of the particles with a mean horizontal velocity $v_0 x/z$.

Equation (9) contains the key idea of this work which is to retrieve the fluid mean velocity of a given flow from a set of trajectories with biased velocities because of tracer concentration gradients. With positive delay $\Delta\tau > 0$, there is no velocity bias and the tracer mean velocity $\mathcal{V}_x(x,z|\Delta\tau > 0)$ is the mean flow velocity, which is $V_x(x,z) = 0$ in this simple toy model.

Without time delay, there is a factor $1/2$ in the horizontal velocity because the velocity estimation involves the position immediately before and immediately after the bin. Equation (8) is simply the average of Eqs. (7) and (9). The solution (8) is used for the model in Fig. 1(b) and it shows a good agreement with the velocity computed from the simulated trajectories without time-delay ($\Delta\tau = 0$).

The method we propose consists in using Eq. (6) to compute Eulerian mapping from a set of particles trajectories. It is referred as a time-delay method because the flow reconstruction uses the information of the position at time t and the velocity at a delayed time $t + \Delta\tau$. Figure 3 represents the implementation of this method for a positive time delay with a trajectory component $x(t)$. In practice for a sample signal with the position and velocity over time, the implementation of the time

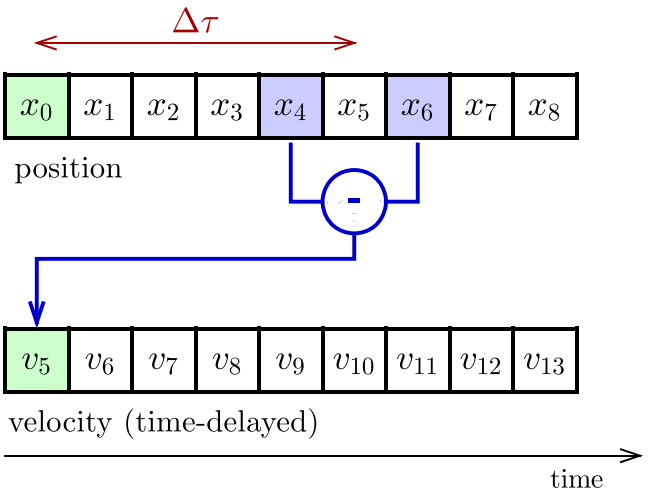

FIG. 3. Representation of the time-delay method on a time signal at a sample rate δt^{-1}. The minus $(-)$ is the two-point velocity operator at location i: $(x_{i+1} - x_{i-1})/2\delta t$. In this example, the velocity is time delayed with $\Delta\tau = +5\,\delta t$ which means that the velocity v_5 is associated to the position x_0. We use the short notation $x_i = x(t_0 + i\,\delta t)$ and $v_i = v(t_0 + i\,\delta t)$ in which t_0 is the reference time for x_0.

delay method consist in removing a the n first velocity points and removing the n last position points ($n = 5$ in the example of Fig. 3). n defines the time delay via the acquisition sampling rate.

III. TIME-DELAYED VELOCITY WITH TURBULENT FLOWS

The point of this paper is to show how time-delayed velocity (6) can be used to suppress the bias caused by nonhomogeneous seeding in a particle tracking experiment. In the toy model previously discussed, any strictly positive delay $\Delta\tau > 0$ gives the correct mean flow $V_x(x, z) = 0$. In the following, we will investigate how the time-delay method applies for a turbulent channel (numerical simulation) and a turbulent jet (experimental results). We will notably investigate the impact of the value $\Delta\tau$ on the determination of the mean flow characteristics.

A. Channel flow

The time-delay analysis is first tested for a simulated particle tracking experiment in a channel flow. To do so, we use the Turbulent Channel Flow data set from the Johns Hopkins Turbulence Databases [40–42].

The channel has a rectangular cross section with rigid walls at $y = -1$ and $y = 1$ and periodic boundary conditions for x and z. The flow is forced in the z direction by an imposed pressure gradient such that the mean velocity equals one. The kinematic viscosity is 5×10^{-5} and the simulation time step is 0.0013. The flow is in the turbulent regime with a Taylor-microscale Reynolds number $\mathrm{Re}_\lambda \approx 344$. Figure 4(a) shows a snapshot of the axial velocity in the range $0 < z < 10$ with $x = 0$. The time-averaged velocity $V_z(x, y, z)$ is represented on top of the contour. For the mean transverse velocities, there is no mean flow $V_x(x, y, z) = 0$ and $V_y(x, y, z) = 0$ because of the confining walls. The mean velocity $V_z(x, y, z)$ is almost independent of the position y in the center of the channel $-0.6 < y < 0.6$. We use the Lagrangian tracking `GetPosition` function [43] that computes the motion of fluid particles from the direct numerical simulation of the channel flow. The obtained trajectories correspond to the motion of ideal tracers virtually injected in the simulated flow. The initial position of 14 000 tracers is set in the middle of the channel. The initial positions for the virtual tracks are set near the line $y = 0, z = 0$ for different values of x and the simulation runs for a duration of 13 time units. We assume that the flow is statistically invariant in x and the initial position

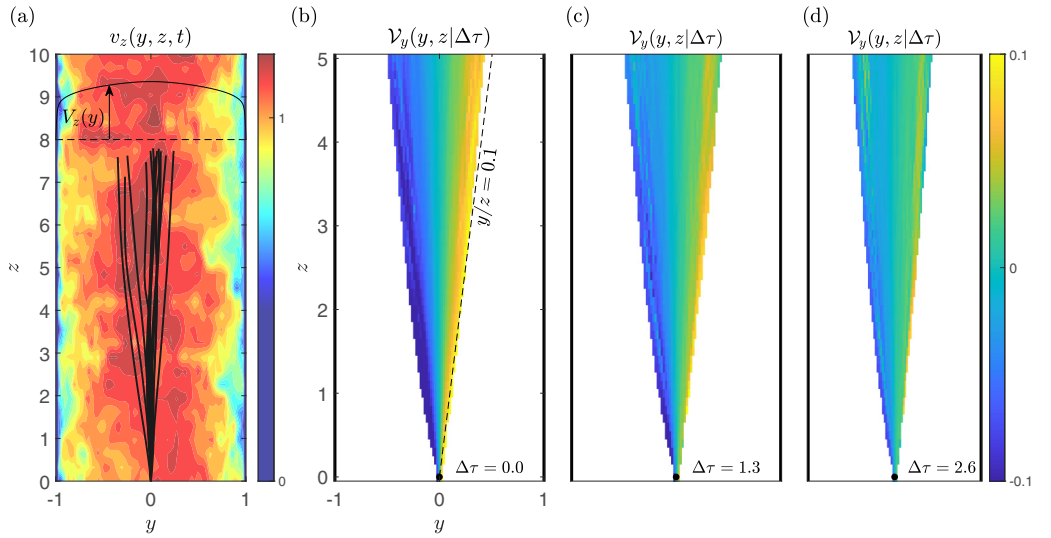

FIG. 4. (a) Instantaneous velocity $v_z(y, z, t)$ for the channel flow simulation ($x = 0$). The rigid walls are at $y = \pm 1$. 15 fluid particle tracks injected at $y = 0$, $z = 0$ are represented by solid lines. (b) Transverse velocity component $\mathcal{V}_y(y, z|\Delta\tau = 0)$ based on tracer tracks with a point source seeding in a turbulent channel flow. Panels (c) and (d) are the transverse velocity maps for two positive values of $\Delta\tau$. $\Delta\tau$ is a time lag introduced between velocity and position in the trajectory analysis.

$X(0)$ of each track is removed to have an effective source-point injection at $x = 0$, $y = 0$, and $z = 0$. We find Eulerian averages (spatial mean statistics) of the Lagrangian based flow field by binning the trajectories in x, y, and z and averaging over the time of the simulation. For the Eulerian contour in Figs. 4(b), 4(c) and 4(d), we use a bin size of $\delta x = 0.02$, $\delta y = 0.02$, and $\delta z = 0.1$. The parameter $\Delta\tau$ is the time delay introduced in the computation of the time-delayed velocity in Eq. (6).

Figure 4(b) shows the mean transverse velocity $\mathcal{V}_y(y, z|\Delta\tau = 0)$ obtained from the analysis of the trajectories computed in the channel flow. The colorbar represents the magnitude of the mean velocity in the transverse direction. The magnitude of the horizontal velocity is of the order of $0.1 \times V_z(y = 0)$ on the side of the cone identified by the dashed line $y/z = 0.1$. The horizontal velocity is twice the velocity bias predicted by the discrete modeling Eq. (8) or equivalently the horizontal velocity matches with the incoming velocity in Eq. (7). This denotes a difference with the toy model presented in section II that we attribute to the existence of a finite correlation timescale for the particle trajectories. For the toy model, there is no correlation time in the trajectory and the velocity without time delay is an average of the position before (with seeding bias) and the position after (without seeding bias) a given point. This average leads to the factor $1/2$ in the velocity without time delay [Eq. (8)]. For the channel flow, the trajectories are smooth at small timescales and the velocity can not be discontinuous. By continuity, the velocity without time delay matches with the incoming velocity immediately before a given position.

Figures 4(c) and 4(d) shows the transverse velocity maps for implementation of time delays $\Delta\tau = 1.3$ and $\Delta\tau = 2.6$, respectively. The transverse velocity decreases with the increase of the time delay. To quantitatively analyze the effect of $\Delta\tau$ on the transverse velocities estimation, the RMS differences of the transverse velocities $\mathcal{V}_x(y, z|\Delta\tau)$ and $\mathcal{V}_y(y, z|\Delta\tau)$ based on the Eulerian flow are represented as a function of the time delay in Fig. 5(a). A value of zero means that the mean flow for the tracers matches with the fluid mean flow [$V_x(x, y, z) = 0$ and $V_y(x, y, z) = 0$ for the channel]. The velocity difference as a function of the time delay approximately follows an exponential decay with a time constant $\tau_c = 2.9$. This means that the time delay between position and velocity in the trajectory analysis has to be typically larger than 2.9 to remove the bias from the point source seeding.

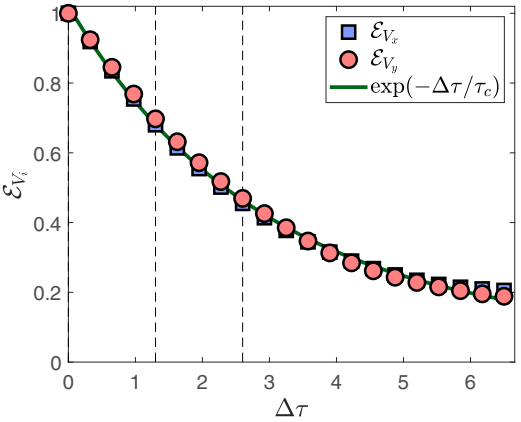

FIG. 5. Magnitude $\mathcal{E}_{V_i}$ of the transverse velocities $\mathcal{V}_i(x, y, z|\Delta\tau)$ with $i = x$ and y as a function of the time delay $\Delta\tau$ in the turbulent channel simulation. $\mathcal{E}_{V_i} = \langle\mathcal{V}_i(y, z|\Delta\tau)\rangle_{y,z}/\langle\mathcal{V}_i(y, z|0)\rangle_{y,z}$ with $\langle.\rangle_{y,z}$ the RMS average over space. $\mathcal{E}_{V_i}$ is a strictly positive quantity that represents the normalized error between the transverse velocities computed from the tracers trajectories $\mathcal{V}_i(y, z|\Delta\tau)$ and the fluid mean velocity $V_x(y, z) = 0$ and $V_y(y, z) = 0$. An exponential fit with a time constant $\tau_c = 2.9$ is represented. The vertical dashed lines indicates the values $\Delta\tau = 1.3$ and 2.6 used in Figs. 4(c) and 4(d).

The timescale τ_c can be interpreted as a memory time of the fluctuating component of the frame of the fluid particles motion. To test this interpretation, we compute the cross correlation signal $\chi_{vv}(\Delta t) = \int v(z = ct, t + \Delta t)v(z = ct, t)dt$ from the transverse velocity component in the frame of the moving fluid. In the center of the channel $|y| < 0.6$ where the particles are injected, the longitudinal velocity is $c = 1.089$, which is slightly larger than the mean velocity. We find a timescale $\tau_\chi = 2.0$. This timescale is of the same order of magnitude than τ_c. This is consistent with the idea that the time delay between position and velocity has to be larger than the memory time of the flow in the frame of the trajectories to remove the bias of the nonhomogeneous seeding.

B. Turbulent jet with nozzle injection

The second implementation of the time delay method is for experimental data with a turbulent jet. A monophasic turbulent round jet is obtained by the injection of water through a nozzle of diameter 4 mm and at a flow rate of the order of 10^{-4} $\mathrm{m^3 s^{-1}}$ into a water tank. The tagging particles are nearly neutrally buoyant polystyrene spheres of typical diameter 0.25 mm and density 1060 $\mathrm{kgm^{-3}}$. The particles are mostly injected from the nozzle so that only the fluid particles coming from the nozzle are tagged. In practice, some polystyrene particles from previous experiments are present in the water tank. The concentration of such pre-existing particles is well below the concentration of the injected particles. An ensemble of trajectories is recorded using a stereoscopic visualization technique at frame rate of 6 kHz with three high-speed cameras. More details about the experimental configuration and the particle tracking method can be found in previous works using the same configuration [15,44].

Figure 6(a) shows a subset of particles trajectories recorded in the turbulent jet. The full set of trajectories is used to construct a Eulerian representation of the mean flow. Figure 6(b) shows the mean axial velocity $\mathcal{V}_z(r, z|0)$ of the jet computed from the trajectory of the particles without time delay (standard particle tracking velocimetry). $\mathcal{V}_z(r, z|0)$ is represented for different z positions identified by dashed lines in Fig. 6(a). The inserted plot is the normalized axial velocity $\overline{\mathcal{V}_z} = \mathcal{V}_z(r, z|0)/\mathcal{V}_z(0, z|0)$ represented as a function of r/z. Here, we approximate the normalized axial velocity $\overline{V_z} = V_z(r, z)/V_z(0, z)$ by a Gaussian [45] function

$$\frac{V_z(r, z)}{V_z(0, z)} = \exp\left(-A\frac{r^2}{z^2}\right), \tag{10}$$

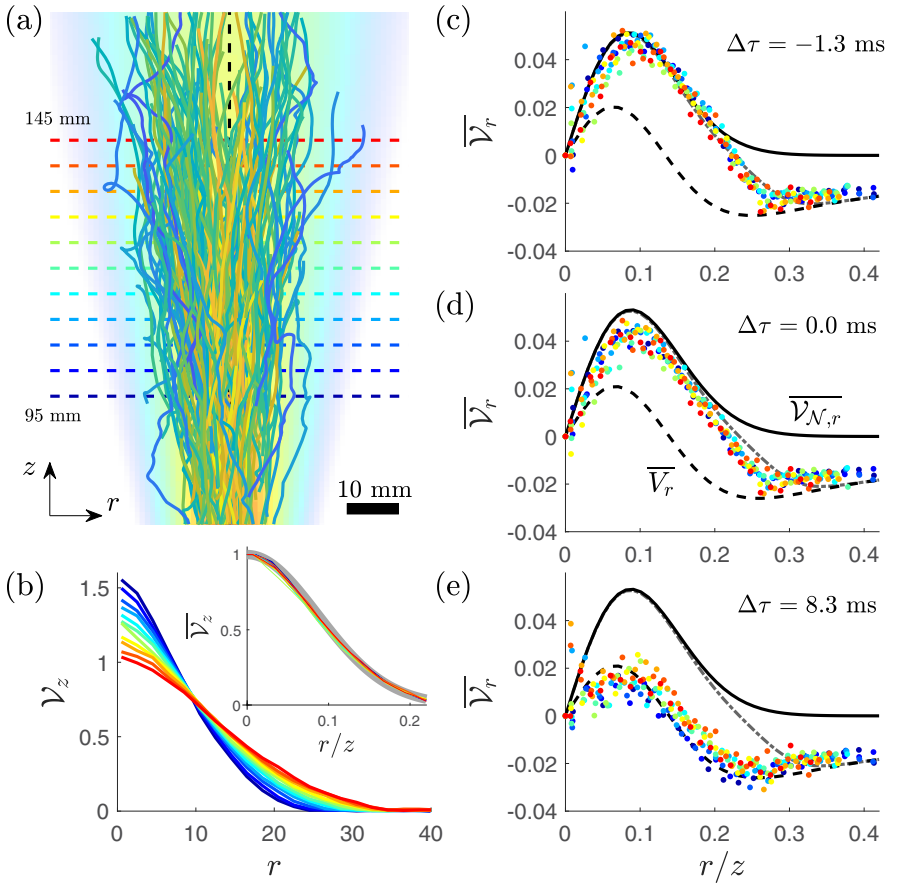

FIG. 6. (a) Particle tracks in a turbulent jet with nozzle injection. The dashed lines mark different distances z to the nozzle chosen to represent the flow profiles. (b) Axial velocity $\mathcal{V}_z$ obtained from the tracks analysis without time delay (standard PTV) as a function of the radial distance r for the 11 positions in z between 95 mm and 145 mm. The velocity at $r = 0$ decreases with increasing z. The inserted plot is the velocity normalized by the velocity at $r = 0$ as a function of the variable r/z. The 11 curves collapse on a master curve corresponding to the Gaussian solution (10) represented by a thick gray line. Panels (c), (d), and (e) are the normalized radial profiles $\overline{\mathcal{V}_r} = \mathcal{V}_r(r, z|\Delta\tau)/\mathcal{V}_z(0, z|\Delta\tau)$ for different values of the time delay $\Delta\tau = -1.3$, 0, and 8.3 ms, respectively. The dashed line is the solution $\overline{V_r} = V_r(r, z)/V_z(0, z)$ for the radial velocity without seeding bias [Eq. (11)]. The solid line is the solution $\overline{\mathcal{V}_{\mathcal{N},r}} = \mathcal{V}_{\mathcal{N},r}(r, z)/\mathcal{V}_{\mathcal{N},z}(0, z)$ for the tracer mean flow for a nozzle seeding [Eq. (12)]. The dash-dotted line is a model $\mathcal{V}_{\mathcal{N}+\mathcal{U},r}(r, z)$ combining nozzle seeding and the contribution of tracers initially in the water tank [Eq. (14)].

in which $A = 67$ is a free dimensionless parameter that relates to the opening angle of the jet. The axial flow tagged by the tracers $\overline{\mathcal{V}_z}$ is in good agreement with the Gaussian model (10). Equation (10) is a usual approximation for the mean axial velocity $\overline{V_z} = V_z(r, z)/V_z(0, z)$ for a turbulent jet. As already discussed in a previous work [15], there is no apparent bias from nonhomogeneous seeding for the axial velocity component in a turbulent jet and then $\overline{\mathcal{V}_z} = \overline{V_z}$.

Figure 6 also represents the normalized radial velocity obtained with three different time-delays with (c) $\Delta\tau = -1.2$ ms, (d) $\Delta\tau = 0$ ms, and (e) $\Delta\tau = 8.3$ ms. The velocities are normalized by the centerline velocities $\mathcal{V}_z(0, z|\Delta\tau)$ and represented as a function of the self-similar coordinate r/z.

Figure 6(e) is the main result of this paper: with a positive time delay $\Delta\tau > 0$, we recover the mean radial flow of the jet $\mathcal{V}_r(r, z|\Delta\tau)/\mathcal{V}_z(0, z|\Delta\tau) = V_r(r, z)/V_z(0, z)$ even if the seeding is

nonhomogeneous. For a turbulent jet, this solution is obtained from the axial solution (10) and the volume continuity equation for an incompressible flow:

$$\frac{V_r(r,z)}{V_z(0,z)} = \frac{r}{z}\exp\left(-A\frac{r^2}{z^2}\right) - \frac{z}{r}\frac{1-\exp\left(-A\frac{r^2}{z^2}\right)}{2A}. \tag{11}$$

This radial solution is represented by dashed lines in Figs. 6(c), 6(d) and 6(e), and it corresponds to the mean radial velocity obtained with homogeneous seeding, meaning the unbiased mean velocity of a turbulent jet.

The radial velocity profile in Fig. 6(d) is without time delay (conventional PTV, $\Delta\tau = 0$). It is clear that the mean radial velocity obtained by the particles trajectories is not the expected solution (11) for the fluid mean velocity or $\mathcal{V}_r(r,z|0)/\mathcal{V}_z(0,z|0) \neq V_r(r,z)/V_z(0,z)$. This is due to the fact that the trajectories recorded at position (r,z) are a subset of the possible fluid trajectories with the condition that the trajectory must come from the nozzle (0,0).

In Figs. 6(c), 6(d) and 6(e), a black solid line is used to represent another solution for the tracer mean radial velocity:

$$\frac{\mathcal{V}_{\mathcal{N},r}(r,z)}{\mathcal{V}_{\mathcal{N},z}(0,z)} = \frac{r}{z}\exp\left(-A\frac{r^2}{z^2}\right). \tag{12}$$

This solution was obtained in a previous work [15] and aims at describing the mean radial velocity of the tracers if the tracers are injected by the nozzle (the subscript $\mathcal{N}$ is for nozzle). If the tracers are injected by the nozzle, then the tracer concentration verifies the same self-similar properties than the axial velocity itself [46], which allows us to compute the solution (12). We can mention that the solution (12) for the radial velocity has a interesting geometrical property:

$$\frac{\mathcal{V}_{\mathcal{N},r}(r,z)}{\mathcal{V}_{\mathcal{N},z}(r,z)} = \frac{r}{z}. \tag{13}$$

The relation (13) means that the particles trajectories are, in average, a set of straight lines with their origin at the nozzle: for any point (r,z), the velocity vector $\mathcal{V}_{\mathcal{N},r}\,\vec{u}_r + \mathcal{V}_{\mathcal{N},z}\,\vec{u}_z$ is aligned with the position vector $r\,\vec{u}_r + z\,\vec{u}_z$. As a consequence, the radial flow $\mathcal{V}_{\mathcal{N},r}$ for the tracers coming from the nozzle is always positive for any r/z.

In the turbulent jet with nozzle injected tracers, we can mention a simple experimental evidence that shows that the mean path of the tracers is not the mean velocity of the fluid. As shown in Fig. 6, the solution (11) for the fluid radial velocity $V_r(r,z)/V_z(0,z)$ is negative for large r/z ($r/z > 0.14$). A negative $V_r(r,z)$ for large r/z means that the outer fluid is entrained by the core of the jet and the mean flow is radially convergent for $r/z > 0.14$. If the tracers were following the mean radial flow V_r, then there would be no possibility for the tracers in region $r/z < 0.14$ to reach the region $r/z > 0.14$. This is not what is experimentally observed. To allow the tracers to be spread by the jet and reach $r/z > 0.14$, the tracers flow $\mathcal{V}_{\mathcal{N},r}(r,z)$ is consistently positive for any r/z and $\mathcal{V}_r(r,z) > V_r(r,z)$ is a signature of a positive radial dispersion of the tracers from the nozzle because of the turbulent diffusion.

In Fig. 6(d), the mean radial velocity $\mathcal{V}_r(r,z|0)$ is consistently larger than $V_r(r,z)$. However, the radial flow $\mathcal{V}_r(r,z|0)$ does not strictly match with the expected solution (12) predicted for tracers injected by the nozzle. We propose that the difference between the model $\mathcal{V}_{\mathcal{N},r}(r,z)$ and the data $\mathcal{V}_r(r,z|0)$ for small r/z comes from the finite size of the filtering kernels used to obtain the velocity from the trajectories. To obtain the velocity at a given time step t_0, we use a two-point derivative estimation combined with a Gaussian filtering. The Gaussian kernel has a window size of 12 time points which means that a few points before and after t_0 are involved in the computation of the velocity. At a frame rate of 6 kHz, six time points for the half window corresponds to 1 ms. Consistently, the agreement between the solution (12) is further improved, at least for small to moderate r/z values, if the velocity $\mathcal{V}_r(r,z|\Delta\tau)$ has a negative delay of $\Delta\tau = -1.3$ ms as shown in Fig. 6(c). This can be interpreted as an optimal realization of the nozzle seeding condition.

In Fig. 6(c), the experimental data deviates from the solid line $\overline{V_{\mathcal{N},r}}$, typically for $r/z > 0.25$. We interpret that this deviation comes from the few unwanted particles that might have remained in the tank from a previous experiment. We should insist on the fact that for r/z typically larger than 0.25, the concentration of particles coming from the nozzle is very low. As mentioned before, the particle concentration is proportional to the axial velocity. It can be verified in Fig. 6 that the axial velocity, and thus the particle concentration that comes from the nozzle, is indeed very small [$\propto \exp(-Ar^2/z^2)$] when r/z is sufficiently large. Consequently, a very small quantity of pre-existing particles can significantly bias the velocity profile with nozzle conditioning, at least far from the axis. A third model $\mathcal{V}_{\mathcal{N}+\mathcal{U},r}$ for the radial velocity is proposed in Fig. 6 that sums the weighted contribution of the tracers coming from the nozzle ($\mathcal{N}$) and the unwanted tracers ($\mathcal{U}$) initially in the water tank

$$\mathcal{V}_{\mathcal{N}+\mathcal{U},r}(r,z) = \frac{\phi(r,z)\mathcal{V}_{\mathcal{N},r}(r,z) + \phi_i V_r(r,z)}{\phi(r,z) + \phi_i}, \tag{14}$$

in which $\phi(r,z) = \phi_0 \exp(-Ar^2/z^2)$ accounts for the tracer concentration in the Gaussian approximation with ϕ_0 the concentration magnitude. ϕ_i is the initial concentration of tracers. The model in Figs. 6(c), 6(d) and 6(e) is for $\phi_i/\phi_0 = 8 \times 10^{-3}$. We assume that the concentration of unwanted tracers initially in the tank is homogeneous, which means that the contribution from ϕ_i is the unbiased jet velocity $V_r(r,z)$.

One could ask about the different delays used to match the two solutions (11) and (12) (-1.3 ms and 8.3 ms). To match the trajectory path solution, the trajectory analysis only needs to remove the position immediately after a given time t. In our track analysis, we use a Gaussian kernel for filtering with a characteristic length of 1 ms for both the position and the velocity. Therefore, a delay of -1.3 ms means that only the past of the trajectory is involved in the velocity estimation at a given time point. To match the normalized velocity $\overline{V_r}$ of the fluid represented by the dashed line in Fig. 6, a time-delay of the order of 8 ms is needed. This time should be interpreted as a characteristic correlation time for the fluid velocity.

To investigate in more details the role of the fluid correlation time, $\Delta\tau$ is systematically varied in the case of the delayed velocity ($\Delta\tau > 0$). In Fig. 7(a), the RMS difference between the normalized radial velocity $\mathcal{V}_r(r,z|\Delta\tau)/\mathcal{V}_z(0,z|\Delta\tau)$ and the Gaussian model for the radial velocity $V_r(r,z)/V_z(0,z)$ is computed. In Fig. 7(b), the difference is represented for the normalized axial velocity $\mathcal{V}_z(r,z|\Delta\tau)/\mathcal{V}_z(0,z|\Delta\tau)$. The obtained quantities $\mathcal{E}_{\mathcal{V}_r}$ and $\mathcal{E}_{\mathcal{V}_z}$ quantify the error between the tracer mean velocity and the real fluid velocity and these errors are represented for different positions in the jet and for values of $\Delta\tau$ between 0 ms and 25 ms. For the radial velocity, the agreement with the Gaussian model $V_r(r,z)/V_z(0,z)$ is optimal for $\Delta\tau$ of the order of 5 to 10 ms. For each bin cell at a position z, the minimum for $\langle \mathcal{V}_r(r,z|\Delta\tau)/\mathcal{V}_z(0,z|\Delta\tau) - V_r(r,z)/V_z(0,z)\rangle_r$ is indicated by a cross. The optimal value for $\Delta\tau$ to minimize $\mathcal{E}_{\mathcal{V}_r}$ tends to increase with increasing z which means that larger time delays need to be used for compensated velocity measurements performed far from the nozzle. To validate this statement, we can mention the dependence of the Lagrangian timescale with z for turbulent jets. The Lagrangian timescale is given by $T_{L_z} = \int_0^\infty R_{u_z u_z}(t)dt/R_{u_z u_z}(0)$ in which $R_{u_z u_z}(t) = \langle \mathcal{V}_z(t_0+t)\mathcal{V}_z(t_0)\rangle$ with $\mathcal{V}_z$ is the Lagrangian velocity of the fluid along the z direction and $\langle . \rangle$ denotes an average over the particle trajectories. For an exponential decay of the Lagrangian velocity correlations $R_{u_z u_z}(t) \propto \exp(-t/t_e)$, T_{L_z} is simply the time constant t_e. The Lagrangian timescale relates to the turbulent diffusivity [47] with $K_{\text{turb}} \sim {\sigma_u}^2 T_L$, in which σ_u is the magnitude of the velocity fluctuations. For turbulent jets, the Lagrangian time T_{L_z} increases with the distance z to the nozzle. The two square data points T_{L_z} added in Fig. 7(a) are two Lagrangian times measured for the same experimental configuration in a previous work [44] using a statistical analysis of the tracer trajectories. The fact that the time delay needed to retrieve the mean flow is of the same order than the Lagrangian time is consistent with the results for the turbulent channel presented in Fig. 5. The black dashed line is a guideline $z \propto \sqrt{\Delta\tau}$. This relation is obtained by assuming that the magnitude of the jet D sets a scaling relation between the space and the timescales. The

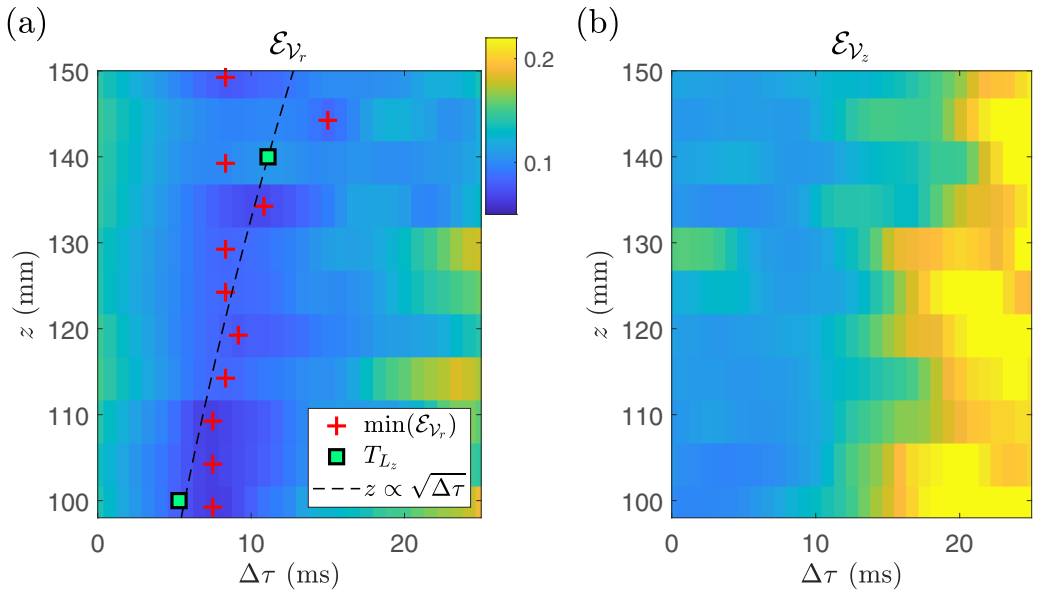

FIG. 7. (a) Error $\mathcal{E}_{\mathcal{V}_r}$ between the normalized radial velocity $\overline{\mathcal{V}_r}$ from the tracers and the jet radial flow in the Gaussian approximation $\overline{V_r}$ (11) as function of the distance to the nozzle z and the time delay $\Delta\tau$. The crosses indicate local minima of $\mathcal{E}_{\mathcal{V}_r}$ for each value of z. The data points T_{L_z} are for Lagrangian timescales computed by statistical analysis of the particles trajectories [44]. (b) Error $\mathcal{E}_{\mathcal{V}_z}$ between the normalized axial velocity $\overline{\mathcal{V}_z}$ and the prediction in the Gaussian approximation $\overline{V_z}$ (10). We define $\mathcal{E}_{\mathcal{V}_i} = \langle \overline{\mathcal{V}_i} - \overline{V_i} \rangle_r$ with $\overline{\mathcal{V}_i} = \mathcal{V}_i(r, z|\Delta\tau)/\mathcal{V}_z(0, z|\Delta\tau)$, $\overline{V_i} = V_i(r, z)/V_z(0, z)$. $\langle . \rangle_i$ is the RMS average over the space coordinate $i = r$ or z.

magnitude of the jet is found in expression for the axial velocity of the jet $V_z(0, z) = D/z$ and it has the dimension of a diffusion coefficient.

For the axial velocity in Fig. 7(b), the agreement with the Gaussian model is not improved with a strictly positive time delay. Standard PTV ($\Delta\tau = 0$) is therefore valid to estimate the axial velocity of the jet $V_z(r, z)$.

Both $\mathcal{V}_r(r, z|\Delta\tau)/\mathcal{V}_z(0, z|\Delta\tau)$ and $\mathcal{V}_z(r, z|\Delta\tau)/\mathcal{V}_z(0, z|\Delta\tau)$ deviate from the Gaussian jet profiles for $\Delta\tau$ typically larger than 20 ms. For the turbulent channel, the mean flow is independent of the mean flow direction z and there is not such deviation for large $\Delta\tau$ as shown in Fig. 5(a). Because the mean flow of the jet is a function of space and notably of z, too large time-delays mean that the velocity is taken too far from the position of a given binning cell, in a region where the mean velocity is different. We can estimate this effect by computing the mean trajectory $Z(t)$ of a set of particles moving on the axis of the jet,

$$V_z(0, Z) = \frac{dZ}{dt} = \frac{D}{Z}, \tag{15}$$

in which D has the dimension of a diffusion coefficient and relates to the magnitude of the jet. After integration over a time delay $\Delta\tau$, we have the mean trajectory of the tracers,

$$Z = \sqrt{{Z_0}^2 + 2D\Delta\tau}, \tag{16}$$

and the mean velocity of the tracers is

$$\mathcal{V}_z(0, Z_0, \Delta\tau) = \frac{D}{Z_0} \frac{1}{\sqrt{1 + \frac{2D\Delta\tau}{{Z_0}^2}}}. \tag{17}$$

This relation means that, even in the absence of seeding bias, using a time delay too large leads to a systematic error caused by the fact the mean velocity field is a function of space. For the distance

$Z_0 = 0.1\,\mathrm{m}$ and a mean velocity at Z_0 equals to $2\mathrm{ms}^{-1}$, we have $D = 0.2\,\mathrm{m}^2\mathrm{s}^{-1}$ and we find a characteristic timescale ${Z_0}^2/2D = 25\,\mathrm{ms}$. In Fig. 7(b), the error $\mathcal{E}_{\mathcal{V}_z}$ between the normalized axial velocity and the model is visible with the time delay approaching 20 ms, which is consistent with the order of magnitude of the timescale ${Z_0}^2/2D = 25\,\mathrm{ms}$. We should however mention that Fig. 7 uses velocities normalized by the centerline velocity D/z. A more accurate analysis should also take into account the radial dependence of the mean flow to fully determine the mismatch caused by the mean flow spatial dependence. However, we assume that, given the geometric properties of turbulent jets, the timescale ${Z_0}^2/2D$ is also relevant regarding the radial dependence of the velocity profiles.

IV. CONCLUSION

In this work, we present a strategy to suppress the bias caused by nonhomogeneous seeding in particle tracking that affects the determination of mean flow velocities.

We first discussed a simplified picture of turbulent diffusion in the form of an advection–diffusion process with a discrete walk of particles. This model was solved analytically for particles injected from a point source and a purely diffuse transverse mean flow was found. The value of the transverse flow in a given observation point has a simple geometrical interpretation related to the relative location of the source point. In this discrete model, the velocity is computed by a position increment. Because of nonsmooth trajectories, we identified that the choice for the definition of the velocity has a crucial impact of the velocity at a given position depending if the position immediately before or immediately after is involved. In the context of this work, the case of interest is the so-called outcoming velocity with the velocity at a given position computed with the position immediately after, which eliminates the bias caused by the source-point seeding.

We then addressed the case of realistic flows with the simulation results of a turbulent channel and the particle dispersion in an experiment with a turbulent round jet. We introduced a time-delayed velocity that allows us to associate, for a given particle trajectory, the position at time t with the velocity at time $t + \Delta\tau$. This time-delayed velocity is the generalization of the outcoming velocity presented in the discrete model that provides unbiased mean flows. Contrary to the discrete model, we found that the time delay $\Delta\tau$ has to be large enough to suppress any velocity bias due to inhomogeneous seeding. For the channel flow, we found that the time delay has to be of the order of a characteristic time that corresponds to a decorrelation time of the velocity in the moving frame of the channel mean flow. For the turbulent jet, the expected radial mean flow is also found with positive time delays but the time delay that has to be introduced increases with the distance to the nozzle. Contrary to the channel flow, there is a limited range for the time delay in the turbulent jet configuration because turbulent jets have a spatial dependence for their mean flow.

The time-delayed velocity method presented here allows the retrieval of the expected mean flow with a nonhomogeneous tracers concentration. The method was tested for two flows of simple geometry and it effectively works with the time delay of the order of a Lagrangian fluid correlation time. The channel flow is a case study for which the compensation method is valid for time delays even larger than the Lagrangian correlation time because there is almost no spatial dependence of the mean flow, notably in the middle part of the channel. Our compensation method also works for turbulent jets, which are open shear flows that notoriously produce strong velocity gradients. In spite of this spatial dependence of the mean flow, a range of time delay is accessible to compensate the bias from inhomogeneous seeding. This suggest that this compensation method with time delays is robust for any type of flows with a well defined mean flow component $V_i(x, y, z)$. We should mention that for unsteady flows, i.e., flows with large scales slowly varying in time, new timescales may be introduce which may limit the applicability of our compensation method.

ACKNOWLEDGMENT

T.B., M.G., and M.B. are supported by the French Research Program No. ANR-13-BS09-0009 ‘LTIF’. B.V., R.V., and M.B. benefit from the financial support of the Project IDEXLYON of the

University of Lyon in the framework of the French Programme Investissements d'Avenir (ANR-16-IDEX-0005). B.V. and R.B.C. are supported by U.S. National Science Foundation Grant No. NSF-GEO-1756259. R.B.C. is also grateful for the support provided through the Fulbright Scholar Program. The authors thank Nicolas Mordant for helpful discussions.

[1] R. J. Adrian, Scattering particle characteristics and their effect on pulsed laser measurements of fluid flow: Speckle velocimetry vs particle image velocimetry, Appl. Opt. **23**, 1690 (1984).
[2] C. J. D. Pickering and N. A. Halliwell, Laser speckle photography and particle image velocimetry: Photographic film noise, Appl. Opt. **23**, 2961 (1984).
[3] R. J. Adrian and J. Westerweel, *Particle Image Velocimetry*, 30 (Cambridge University Press, Cambridge, UK, 2011)
[4] A. A. Adamczyk and L. Rimai, 2-dimensional particle tracking velocimetry (PTV): Technique and image processing algorithms, Exp. Fluids **6**, 373 (1988).
[5] H. G. Maas, A. Gruen, and D. Papantoniou, Particle tracking velocimetry in three-dimensional flows, Exp. Fluids **15**, 133 (1993).
[6] N. T. Ouellette, H. Xu, and E. Bodenschatz, A quantitative study of three-dimensional Lagrangian particle tracking algorithms, Exp. Fluids **40**, 301 (2006).
[7] O. G. Bakunin, *Turbulence and Diffusion: Scaling versus Equations* (Springer Science & Business Media, Cham, 2008).
[8] D. Schanz, S. Gesemann, and A. Schröder, Shake-the-box: Lagrangian particle tracking at high particle image densities, Exp. Fluids **57**, 70. (2016).
[9] R. Mei, Velocity fidelity of flow tracer particles, Exp. Fluids **22**, 1 (1996).
[10] H. Xu and E. Bodenschatz, Motion of inertial particles with size larger than Kolmogorov scale in turbulent flows, Physica D **237**, 2095 (2008).
[11] M. F. Kerho and M. B. Bragg, Neutrally buoyant bubbles used as flow tracers in air, Exp. Fluids **16**, 393 (1994).
[12] A. Melling, Tracer particles and seeding for particle image velocimetry, Meas. Sci. Technol. **8**, 1406 (1997).
[13] S. Ferrari, M. G. Badas, A. Besalduch L, and G. Querzoli, A feature tracking velocimetry technique applied to inclined negatively buoyant jets, in *Proceedings of the 17th International Symposia on Applications of Laser Techniques to Fluid Mechanics* (Instituto Superior Técnico, Lisbon, Portugal, 2014), pp. 1–12.
[14] F. J. W. A. Martins, J. Kirchmann, A. Kronenburg, and F. Beyrau, Quantification and mitigation of PIV bias errors caused by intermittent particle seeding and particle lag by means of large eddy simulations, Meas. Sci. Technol. **32**, 104006 (2021).
[15] T. Basset, B. Viggiano, T. Barois, M. Gibert, N. Mordant, R. B. Cal, R. Volk, and M. Bourgoin, Entrainment, diffusion and effective compressibility in a self-similar turbulent jet, J. Fluid Mech. **947**, A29 (2022).
[16] J. M. Ottino and S. Wiggins, Introduction: Mixing in microfluidics, Philos. Trans. A Math. Phys. Eng. Sci. **362**, 923 (2004).
[17] G. M. Whitesides, The origins and the future of microfluidics, Nature (London) **442**, 368 (2006).
[18] G. K. Batchelor, Diffusion in free turbulent shear flows, J. Fluid Mech. **3**, 67 (1957).
[19] J. W. Elder, The dispersion of marked fluid in turbulent shear flow, J. Fluid Mech. **5**, 544 (1959).
[20] I. B. Goldman and J. M. Marchello, Turbulent schmidt numbers, Int. J. Heat Mass Transf. **12**, 797 (1969).
[21] G. T. Csanady, *Turbulent Diffusion in the Environment*, Vol. 3 (Springer Science & Business Media, Cham, 1973).
[22] R. Woo and A. Ishimaru, Eddy diffusion coefficient for the atmosphere of venus from radio scintillation measurements, Nature (London) **289**, 383 (1981).
[23] F.-J. Lübken, U. Von Zahn, E. V. Thrane, T. Blix, G. A. Kokin, and S. V. Pachomov, In situ measurements of turbulent energy dissipation rates and eddy diffusion coefficients during map/wine, J. Atmos. Terr. Phys. **49**, 763 (1987).

[24] R. Wilson, Turbulent diffusivity in the free atmosphere inferred from MST radar measurements: A review, in *Annales Geophysicae*, Vol. 22 (Copernicus GmbH, Gottingen, 2004), pp. 3869–3887.
[25] S. Businger, S. R. Chiswell, W. C. Ulmer, and R. Johnson, Balloons as a Lagrangian measurement platform for atmospheric research, J. Geophys. Res.: Atmos. **101**, 4363 (1996).
[26] S. Wiggins, The dynamical systems approach to Lagrangian transport in oceanic flows, Annu. Rev. Fluid Mech. **37**, 295 (2005).
[27] J. H. LaCasce, Statistics from Lagrangian observations, Prog. Oceanogr. **77**, 1 (2008).
[28] C. Poulain, N. Mazellier, P. Gervais, Y. Gagne, and C. Baudet, Spectral vorticity and Lagrangian velocity measurements in turbulent jets, Flow, Turbul. Combust. **72**, 245 (2004).
[29] N. M. Qureshi, M. Bourgoin, C. Baudet, A. Cartellier, and Y. Gagne, Turbulent Transport of Material Particles: An Experimental Study of Finite-Size Effects, Phys. Rev. Lett. **99**, 184502 (2007).
[30] S. Ayyalasomayajula, A. Gylfason, L. R. Collins, E. Bodenschatz, and Z. Warhaft, Lagrangian Measurements of Inertial Particle Accelerations in Grid Generated Wind Tunnel Turbulence, Phys. Rev. Lett. **97**, 144507 (2006).
[31] J. Wei and Y. Li, Enhanced spread of expiratory droplets by turbulence in a cough jet, Build. Sci. **93**, 86 (2015).
[32] Y. A. Hassan and R. E. Canaan, Full-field bubbly flow velocity measurements using a multiframe particle tracking technique, Exp. Fluids **12**, 49 (1991).
[33] F. Ravelet, C. Colin, and F. Risso, On the dynamics and breakup of a bubble rising in a turbulent flow, Phys. Fluids **23**, 103301 (2011).
[34] S. Perrard, A. Rivière, W. Mostert, and L. Deike, Bubble deformation by a turbulent flow, J. Fluid Mech. **920**, A15(2021).
[35] S. G. Huisman, T. Barois, M. Bourgoin, A. Chouippe, T. Doychev, P. Huck, C. E. B. Morales, M. Uhlmann, and R. Volk, Columnar structure formation of a dilute suspension of settling spherical particles in a quiescent fluid, Phys. Rev. Fluids **1**, 074204 (2016).
[36] E. W. Saw, R. A. Shaw, S. Ayyalasomayajula, P. Y. Chuang, and A. Gylfason, Inertial Clustering of Particles in High-Reynolds-Number Turbulence, Phys. Rev. Lett. **100**, 214501 (2008).
[37] J. P. L. C. Salazar, J. De Jong, L. Cao, S. H. Woodward, H. Meng, and L. R. Collins, Experimental and numerical investigation of inertial particle clustering in isotropic turbulence, J. Fluid Mech. **600**, 245 (2008).
[38] R. Monchaux, M. Bourgoin, and A. Cartellier, Analyzing preferential concentration and clustering of inertial particles in turbulence, Int. J. Multiphase Flow **40**, 1 (2012).
[39] M. A. Yavuz, R. P. J. Kunnen, G. J. F. Van Heijst, and H. J. H. Clercx, Extreme Small-Scale Clustering of Droplets in Turbulence Driven by Hydrodynamic Interactions, Phys. Rev. Lett. **120**, 244504 (2018).
[40] E. Perlman, R. Burns, Y. Li, and C. Meneveau, Data exploration of turbulence simulations using a database cluster, in *Proceedings of the ACM/IEEE Conference on Supercomputing* (IEEE, 2007), pp. 1–11.
[41] Y. Li, E. Perlman, M. Wan, Y. Yang, C. Meneveau, R. Burns, S. Chen, A. Szalay, and G. Eyink, A public turbulence database cluster and applications to study Lagrangian evolution of velocity increments in turbulence, J. Turbul. **9**, N31 (2008).
[42] J. Graham, K. Kanov, X. I. A. Yang, M. Lee, N. Malaya, C. C. Lalescu, R. Burns, G. Eyink, A. Szalay, R. D. Moser *et al.*, A web services accessible database of turbulent channel flow and its use for testing a new integral wall model for LES, J. Turbul. **17**, 181 (2016).
[43] H. Yu, K. Kanov, E. Perlman, J. Graham, E. Frederix, R. Burns, A. Szalay, G. Eyink, and C. Meneveau, Studying Lagrangian dynamics of turbulence using on-demand fluid particle tracking in a public turbulence database, J. Turbul. **13**, N12 (2012).
[44] B. Viggiano, T. Basset, S. Solovitz, T. Barois, M. Gibert, N. Mordant, L. Chevillard, R. Volk, M. Bourgoin, and R. B. Cal, Lagrangian diffusion properties of a free shear turbulent jet, J. Fluid Mech. **918**, A25(2021).
[45] S. B. Pope, *Turbulent Flows* (Cambridge University Press, Cambridge, UK, 2000).
[46] D. R. Dowling and P. E. Dimotakis, Similarity of the concentration field of gas-phase turbulent jets, J. Fluid Mech. **218**, 109 (1990).
[47] G. I. Taylor, Diffusion by continuous movements, Proc. London Math. Soc. **s2-20**, 196 (1922).